Interfacing transitions of different alkali atoms and telecom bands using one narrowband photon pair source

Schunk, Gerhard; Vogl, Ulrich; Strekalov, Dmitry V.; Förtsch, Michael; Sedlmeir, Florian; Schwefel, Harald G L; Göbelt, Manuela; Christiansen, Silke; Leuchs, Gerd; Marquardt, Christoph

optica

Interfacing transitions of different alkali atoms and telecom bands using one narrowband photon pair source

Gerhard Schunk,[1,2,3,7] **Ulrich Vogl,**[1,2] **Dmitry V. Strekalov,**[1,2] **Michael Förtsch,**[1,2,3] **Florian Sedlmeir,**[1,2,3]
Harald G. L. Schwefel,[1,2,4] **Manuela Göbelt,**[1] **Silke Christiansen,**[1,5] **Gerd Leuchs,**[1,2] **and**
Christoph Marquardt[1,2,6,*]

[1]*Max Planck Institute for the Science of Light, Günther-Scharowsky-Straße 1/Building 24, 90158 Erlangen, Germany*
[2]*Institute for Optics, Information and Photonics, University Erlangen-Nürnberg, Staudtstr. 7/B2, 90158 Erlangen, Germany*
[3]*SAOT, School in Advanced Optical Technologies, Paul-Gordan-Str. 6, 91052 Erlangen, Germany*
[4]*Department of Physics, University of Otago, 730 Cumberland Street, Dunedin 9016, New Zealand*
[5]*Helmholtz Center Berlin for Materials and Energy, Hahn-Meitner Platz 1, 14109 Berlin, Germany*
[6]*Department of Physics, Technical University of Denmark, Building 309, 2800 Lyngby, Denmark*
[7]*e-mail: Gerhard.Schunk@mpl.mpg.de*
Corresponding author: Christoph.Marquardt@mpl.mpg.de

Quantum information technology strongly relies on the coupling of optical photons with narrowband quantum systems, such as quantum dots, color centers, and atomic systems. This coupling requires matching the optical wavelength and bandwidth to the desired system, which presents a considerable problem for most available sources of quantum light. Here we demonstrate the coupling of alkali dipole transitions with a tunable source of photon pairs. Our source is based on spontaneous parametric downconversion in a triply resonant whispering gallery mode resonator. For this, we have developed novel wavelength-tuning mechanisms that allow a coarse tuning to either the cesium or rubidium wavelength, with subsequent continuous fine-tuning to the desired transition. As a demonstration of the functionality of the source, we performed a heralded single-photon measurement of the atomic decay. We present a major advance in controlling the spontaneous downconversion process, which makes our bright source of heralded single photons now compatible with a plethora of narrowband resonant systems.   © 2015 Optical Society of America

1. INTRODUCTION

Photon pairs and heralded single photons are key prerequisites for many schemes in quantum information processing [1,2]. Making their central frequency and bandwidth compatible to the resonances of other physical systems enables a variety of applications, such as efficient quantum memories [3,4], photon–phonon interactions [5], and coupling single photons or squeezed light with single atoms [6] or atomic ensembles [7,8]. It also provides the technology for quantum repeater schemes [9] that are proposed to enhance long-distance quantum communication [10,11].

Presently available single-photon sources [12] do not provide quantum mechanically pure single-mode optical states with high tunability in wavelength and bandwidth. Previously we reported a source based on spontaneous parametric downconversion (SPDC) in an optical resonator operating in a single-mode regime [13], and providing tunable bandwidth [14] compatible with atomic transitions. Here we demonstrate the tuning of the signal

photon wavelength to the rubidium and cesium transitions, whereas the idler photon matches a telecom wavelength.

Spontaneous nonlinear conversion in $\chi^{(2)}$ [14–22] and $\chi^{(3)}$ materials [23,24] offers correlated photon pairs with widely tunable wavelengths, in contrast to many other sources of single photons such as single atoms [25–27], single molecules [28,29], solid-state quantum dots [30–32], or four-wave mixing in atomic ensembles [33–35]. The challenge is to make spontaneous nonlinear conversion both continuously tunable and narrowband to be compatible with quantum memories.

To achieve this, we use a triply resonant cavity. This scheme increases the efficiency of spontaneous nonlinear conversion processes and provides a narrow bandwidth of the cavity in use. Continuous tuning of the output bandwidth in a triply resonant whispering gallery mode resonator (WGMR) is possible [14] by changing the outcoupling rates. Recently, we showed single-mode operation [13] in such a system based on the highly restrictive phase-matching conditions of the triply resonant cavity.

In this work, we demonstrate novel tuning mechanisms to generate photon pairs matching two different narrowband atomic transitions in the near infrared and telecom bands. We use the tunable signal photons (790–1064 nm) for addressing the atomic transitions and the corresponding idler photons (1064–1630 nm) for heralding at telecom wavelengths. For precise tuning of the signal frequency to the Cs D1 line at 895 nm and the Rb D1 line at 795 nm, we introduce a set of tuning mechanisms based on the mode analysis [36] of the WGMR spectrum at the pump wavelength. Relying solely on temperature tuning, one is limited to discrete solutions of the phase-matching conditions. We show continuous tuning of the signal frequency across the Doppler-broadened absorption line of a Cs D1 hyperfine transition by manipulating the evanescent fields of the pump, signal, and idler with a movable dielectric substrate. This continuous frequency tuning with MHz precision allows heralded single-photon spectroscopy, which we demonstrate at this Cs D1 hyperfine transition.

2. EXPERIMENTAL SCHEME

Our source of single photons [14] and squeezed light [37] is based on natural phase matching [38] in a WGMR with radius $R = 2.5$ mm manufactured from a congruent 5.8% MgO-doped lithium niobate wafer (see Fig. 1). The temperature of the WGMR is controlled at the millikelvin scale with a proportional–integral–derivative lock. As a pump source, we use a frequency-doubled Nd:YAG laser at 532 nm in vertical polarization, which is coupled to the WGMR via a diamond prism (see Fig. 1). We use a second piezo actuator for moving a glass substrate, which is coated with zinc oxide. This allows continuous tuning of the resonance frequencies of the eigenmodes. Alternatively, the dielectric substrate can be replaced with a second diamond prism for analysis of the whispering gallery modes [36].

The solution of Maxwell's equations for WGMRs with azimuthally symmetric geometry [39,40] is characterized by three mode numbers [see Fig. 1(c)]: the azimuthal mode number $m \gg 1$, the radial mode numbers $q \geq 1$, and the angular mode number $p \geq 0$. In the experiment, we analyzed the mode spectrum to
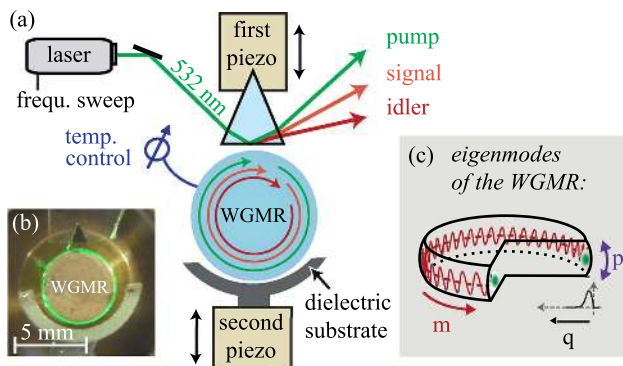
identify the various eigenmodes of the pump, including the fundamental mode with $m_p \approx 64900$, $q_p = 1$, and $p_p = 0$ at a temperature of $T = 140°C$. The loaded quality factor at critical coupling and the free spectral range (FSR) of the fundamental mode were measured to be $Q = 1.6 \times 10^7$ and FSR = 7.8 GHz, respectively.

3. TUNING MECHANISMS FOR PARAMETRIC DOWNCONVERSION IN A TRIPLY RESONANT WGMR

A. Temperature Tuning

The most efficient conversion channel [41] of our parametric downconversion (PDC) process converts light from the extraordinarily polarized fundamental pump mode to the ordinarily polarized fundamental signal and idler modes with $m_s \gg 1$, $q_s = 1$, $p_s = 0$ and $m_i \gg 1$, $q_i = 1$, $p_i = 0$, respectively. Figure 2(a) shows the measured PDC frequencies of this triply resonant optical parametric oscillator (OPO) pumped above the threshold in a temperature range from 100°C to 140°C along with a numerical simulation of conversion channels for higher-order radial PDC modes. Depending on the temperature, the mode of the fundamental pump defined by m_s is selected for a fixed pump laser wavelength. In this graph, we omit nonrelevant conversion channels for clarity, which may be accessed by considering modes with different p and q values [13,42].

Figures 2(b) and 2(c) show the stepwise tuning behavior of the fundamental conversion channel around the Cs and Rb D1 lines, respectively. These steps originate from the interplay between the discrete eigenresonances and the phase-matching requirements. Phase matching in WGMRs [43] is mainly characterized by

$$\nu_p(T, d) = \nu_s(T, d) + \nu_i(T, d), \tag{1a}$$

and

$$m_p = m_s + m_i, \tag{1b}$$

representing energy and momentum conservation, respectively. The resonance frequencies $\nu_{p,s,i}(T, d)$ depend on the temperature T and the distance d between the WGMR and the dielectric substrate controlled with the second piezo actuator. Equation (1b) is equivalent to the conservation of angular momentum for electronic transitions in atomic physics and explains the stepwise tuning behavior in our case. For small temperature changes, we can assume $\nu_{p,s,i}(T)$ to be linear functions in temperature. If Eqs. (1a) and (1b) are fulfilled for a fixed triplet of modes with $m_{p,s,i}$, $q_{p,s,i}$, and $p_{p,s,i}$ at a given temperature T_0, then phase matching for this mode combination is typically allowed only in a narrow interval, i.e., the phase-matching bandwidth around T_0. The magnitude of the phase-matching bandwidth is determined by the bandwidths of the three modes and the different slopes of $\nu_{p,s,i}(T, d)$. However, phase matching for

$$m_p, m_s, m_i \rightarrow m_p, m_s \pm 1, m_i \mp 1, \tag{2}$$

is allowed according to Eqs. (1a) and (1b) at a temperature of $T \pm \Delta T$ keeping the same pump mode. The temperature steps ΔT are determined by the different slopes of $\nu_{p,s,i}(T)$ and the difference in the respective FSRs of the signal and the idler.

B. Selection of the Pump Mode

For measuring the absolute signal frequency on the MHz scale, we beat the signal with a Ti:sapphire reference laser.

Fig. 1. Experimental setup. (a) Type-I PDC in a z-cut WGMR is performed with a pump beam at 532 nm coupling via a diamond prism on top. A second coupling port can be used for dielectric tuning. Alternatively, the dielectric substrate can be replaced with a second diamond prism for mode analysis [36]. (b) Top view of the WGMR. (c) Illustration of the eigenmodes of WGMRs. These eigenmodes are defined by the azimuthal mode number m, radial mode number q, and angular mode number p.
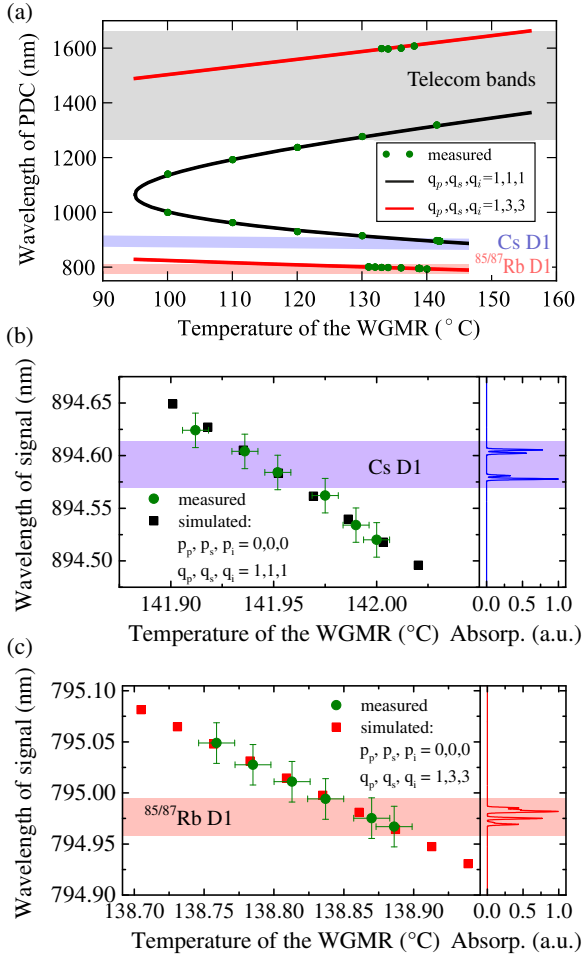
Fig. 2. Temperature tuning of the PDC process in our triply resonant optical parametric oscillator above the pump threshold. The generated signal and idler beams connect various alkali atoms to telecom wavelengths. (a) Emission wavelengths from 790 to 1630 nm are measured for a fundamental pump mode with $m_p \gg 1$, $q_p = 1$, and $p_p = 0$ emitting into various signal and idler mode combinations. We show the branches relevant for tuning to the D1 lines of Cs and $^{85/87}$Rb. (b) Temperature fine-tuning of the fundamental conversion channel $q_p, q_s, q_i = 1, 1, 1$ around the Cs D1 line shows a stepwise tuning behavior keeping the azimuthal mode number m_p of the pump fixed. (c) The same stepwise tuning behavior is found for the nonfundamental conversion channel $q_p, q_s, q_i = 1, 3, 3$ around the $^{85/87}$Rb D1 line. The right panels show the calculated absorption profiles for Cs and $^{85/87}$Rb [45]. The uncertainties shown result from the limited resolution of the optical spectrum analyzer (AQ6370C, Yokogawa).

This reference laser scans over the approximately 500-MHz-wide Doppler-broadened Cs D1 line in a saturated absorption configuration. The beat signal then only appears when the frequency difference between the reference laser and the signal is within the detector bandwidth (PDA36A from Thorlabs with 11 kHz bandwidth). Notably, above the threshold, the bandwidth of parametric light [44] is determined by the pump bandwidth, in contrast to the subthreshold operation when it is determined by the resonator linewidth (see Figs. 4 and 5). The atomic line data for Cs and $^{85/87}$Rb were taken from [45]. By changing the pump mode azimuthal mode number as

$$m_p, m_s, m_i \rightarrow m_p \pm 1, m_s, m_i \mp 1, \qquad (3)$$

we achieve an overall tuning of the signal frequency of approximately 1 GHz in steps of 254 MHz as presented in Fig. 3(a). Notably, the mode numbers $m_s \gg 1$, $q_s = 1$, and $p_s = 0$ of the signal do not change in this process and frequency tuning occurs only due to the temperature-dependent frequency drift of the same signal mode. Using this approach, the complete interval between two steps of about 0.022 nm (corresponding to 8.2 GHz) shown in Figs. 2(b) and 2(c) can be covered if an overall tuning of the pump laser over approximately 240 GHz is provided. Furthermore, all conversion channels that are allowed by the phase-matching conditions can be used for tuning to the desired wavelength, which relaxes the requirements on the pump laser tuning. For example, for our tuning to the Rb D1 line, we used the nonfundamental conversion channel $q_p, q_s, q_i = 1, 3, 3$. Here again we measured the beat signal of the generated signal and the Ti:sapphire reference laser at the Doppler-broadened ^{85}Rb D1 F3′–F2 line.

C. Perturbation of the Evanescent Fields

Triply resonant OPOs offer efficient PDC and narrowband photon pairs under the constraint of the stepwise tuning behavior discussed in the previous section. An addressing of atomic transitions with arbitrary detuning requires continuous frequency adjustments at the MHz scale. We achieve continuous tuning of the phase matching by combining temperature tuning and the effect of a movable dielectric substrate, i.e., a curved glass substrate coated with highly refractive zinc oxide ($n_{ZnO} = 2.03$ at 532 nm [46]) by atomic layer deposition [47], within the evanescent fields of the WGMR [48]. This does not lead to a reduction of the optical quality factor via outcoupling since the refractive index of the WGMR is higher than the refractive index of the dielectric substrate. As all three modes, the pump, signal, and idler, are affected, we adjust the pump laser frequency to the new phase-matching condition. In contrast to changing the mode numbers of the three modes, we change their resonance frequencies by $\delta\nu_{p,s,i}$ while fulfilling the energy conservation requirement given by Eq. (1a). Thereby, the signal frequency ν_s shifts as

$$\delta\nu_s(T, d) = \delta\nu_p(T, d) - \delta\nu_i(T, d). \qquad (4)$$

An increase in the voltage of the second piezo actuator, which changes the distance between the dielectric and the WGMR, in combination with temperature adjustments allows continuous tuning of the signal frequency over approximately 400 MHz as shown in Fig. 3(b). This tuning range exceeds the previously reported value of 150 MHz achieved via the electro-optical effect of lithium niobate [14], which provides an additional method for fast switching.

4. COUPLING SINGLE PHOTONS TO ATOMS

In the previous section, we have shown accurate frequency measurements of the generated parametric beams above the OPO threshold using spectral lines as a reference. In the following text, we directly show light–atom coupling for the desired single-photon states. The single-photon regime [14] in this WGMR-based OPO is reached by reducing the pump power far below the OPO threshold [38,49,50] of 18 μW at a temperature of $T = 141°C$ with signal and idler wavelengths of $\lambda_s = 895$ nm and $\lambda_i = 1312$ nm, respectively. This threshold was measured for the most efficient conversion channel of the PDC process using
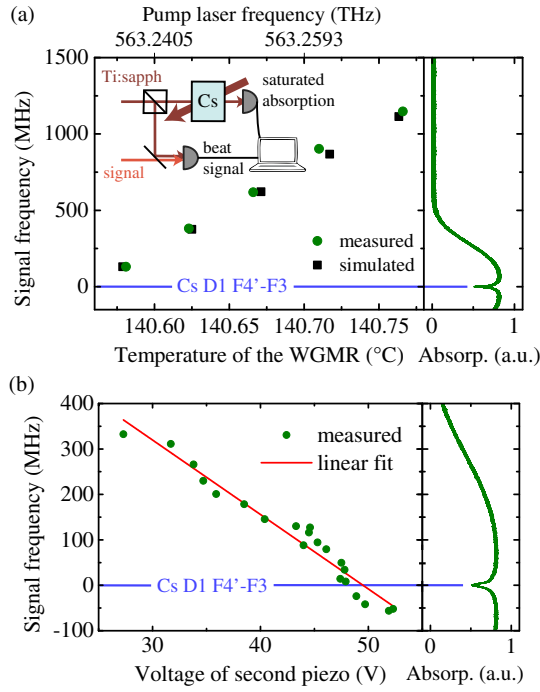
Fig. 3. Frequency tuning of the PDC process measured via a beat signal between the signal beam and the Ti:sapphire reference laser in a saturated absorption configuration. The right panels show the measured Ti:sapphire absorption at the Cs D1 F4'–F3 line, including the Doppler-free dip on resonance. (a) A change in the azimuthal mode number m_p of the pump mode accompanied by a temperature adjustment results in an average change in the signal emission frequency by $\Delta \nu_s = 254$ MHz. (b) Tuning across the Doppler-broadened line is achieved by shifting the resonance frequencies of the pump and the parametric modes with a movable dielectric substrate in the evanescent fields (we estimate the distance change per applied voltage on the actuator to be 15 nm V^{-1}).

Fig. 4. Absorption of the signal light by the atoms. (a) In this measurement, we decreased the pump power below the OPO threshold to demonstrate resonant single photons. The pump laser frequency was locked to the fundamental mode, whereas the WGMR temperature was changed continuously. We measured a suppression of the count rate by $97 \pm 3\%$ at the Cs D1 F4'–F3 line in (a) and $98 \pm 4\%$ at the ^{85}Rb D1 F3'–F2 line in (b). The frequency width of the peaks directly gives the respective phase-matching bandwidths of the PDC process. Images of bright fluorescence in the Cs cell in (c) and the Rb cell in (d) were taken far above the OPO threshold.

fundamental pump, signal, and idler modes with $m_{p,s,i} \gg 1$, $q_{p,s,i} = 1$, and $p_{p,s,i} = 0$.

The phase-matching conditions given by Eqs. (1a) and (1b) determine the threshold of the PDC process and also the efficiency of the SPDC process. The possibility to fulfill energy conservation [Eq. (1a)] for three given modes is highly dependent on the temperature of the WGMR. In Fig. 4, we show the temperature-dependent detuning of the modes from the phase-matching point via the count rates of the signal photons. The idler photons are not considered for this absorption measurement. One half of the signal photon flux is sent through the vapor cells and the other half is directly detected as a reference. APD 1 and APD 2 are Si avalanche photodiodes (SPCM CD 3017 from Perkin Elmer). The cell was 5 cm long and was at a temperature of 80°C. Interference filters (FB900-25 at 900 ± 5 nm from Thorlabs for the Cs D1 line and ASE-797 at 794.979 ± 0.125 nm from Ondax for the Rb D1 line) were used to filter out signal modes that were separated by several nanometers from the desired wavelength.

Below the threshold, it is possible to generate photons in multiple PDC conversion channels at the same time. This aspect cannot be deduced from the above threshold measurements presented in Fig. 3 due to the different working principle of the PDC above the threshold based on self-seeding and the limited
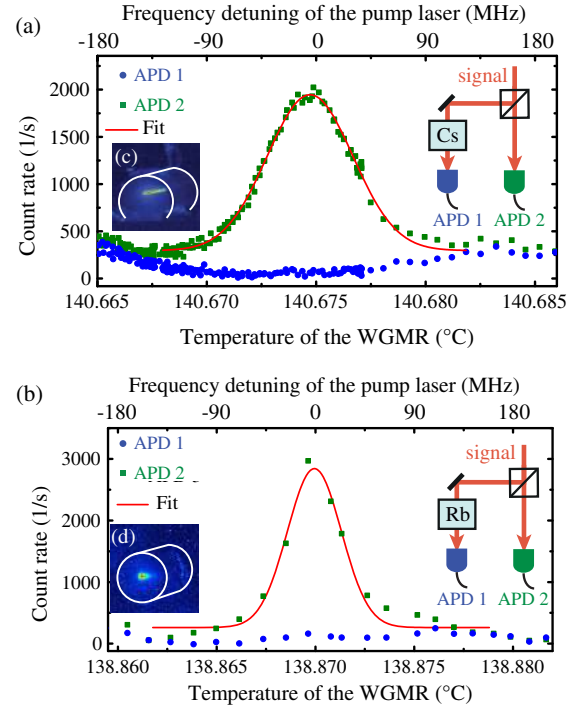
detection range of approximately 2 GHz in the beat signal measurement. However, the high absorption value of $97 \pm 3\%$ for Cs and $98 \pm 4\%$ for Rb shows that all signal photons in this measurement were residing within the approximately 500-MHz-wide Doppler broadening of the alkali atoms. Single-mode operation [13] without an additional bandpass filter occurs if the phase-matching temperatures of the most efficient conversion channels are separated by more than the phase-matching bandwidth. This can in principle be achieved with an adaption of the radius and the curvature of the WGMR.

Next we investigate the temporal correlations of the signal and idler at the single-photon level while the signal photons are interacting with the cesium atoms. The arrival of signal photons is heralded with idler photons detected with APD 3, which is an InGaAs/InP avalanche photodiode (ID220 from ID Quantique). Figure 5(a) shows the measured correlation function $g_{si}^{(2)}(\tau)$ of the directly detected signal and idler photons with a double-exponential fit given by

$$g_{si}^{(2)}(\tau) \propto \frac{1}{2} \cdot \frac{e^{-|\tau|/\tau_{si}}}{\tau_{si}} \quad (5)$$

at a pump power of 0.39 μW. A comparison of the count rate on each APD with the measured coincidences yields a Klyshko efficiency [51] of 1.5% for the idler and 0.9% for the signal. The lower limits for the overall losses are only given by the material
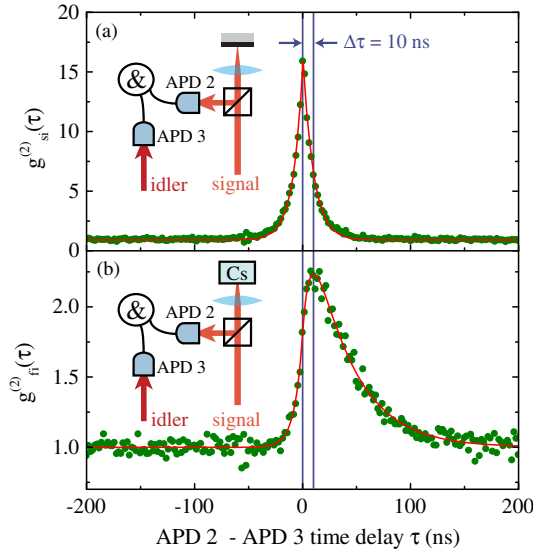
Fig. 5. Photon–atom coupling. (a) The measured coincidences (2 ns bin width, 120 s integration time) from the directly detected signal and idler photons are fitted with the double-exponential function given by Eq. (5). This yields a decay time of $\tau_{si} = 9.4$ ns corresponding to a photon bandwidth of $\gamma_{si} = 16.9$ MHz. (b) This measurement of heralded fluorescence (2 ns bin width, 60 min integration time) allows a direct probing of the atomic decay. The time delay of $\Delta\tau = 10$ ns with respect to the reference measurement in (b) is in agreement with the theoretical model given by Eq. (6).

absorption of lithium niobate, which can be optimized by using crystals of higher optical grade or simply by lowering the decay times by overcoupling the resonator.

The decay times of the signal and idler τ_{si}, i.e., the respective bandwidths $\gamma_{si} = 1/(2\pi \cdot \tau_{si})$, can be tuned jointly by controlling the distance between the coupling prism and the WGMR. We measured a bandwidth tuning of approximately $\gamma_{si} = 6{-}24$ MHz ($\gamma_{si} = 7{-}13$ MHz was shown in Ref. [14]).

Figure 5(b) shows the measured correlation function of directly detected idler photons heralding photons coming from the resonant fluorescence of the Cs D1 F4′–F3 line at a pump power of 3.3 μW. We calculate the correlation function $g_{fi}^{(2)}(\tau)$ for this heralded fluorescence measurement with a stochastic atomic decay model with an exponential probability distribution characterized by an atomic decay time of τ_f:

$$g_{fi}^{(2)}(\tau) \propto \frac{1}{2} \cdot \begin{cases} \dfrac{e^{\tau/\tau_{si}}}{\tau_f + \tau_{si}}, & \tau < 0, \\[2ex] \dfrac{e^{-\tau/\tau_f}}{\tau_f + \tau_{si}} + \dfrac{e^{-\tau/\tau_{si}} - e^{-\tau/\tau_f}}{\tau_{si} - \tau_f}, & \tau > 0. \end{cases} \quad (6)$$

The fit of the heralded correlation function $g_{fi}^{(2)}(\tau)$ in Fig. 5(c) matches the experimental data very well, yielding time constants of $\tau_{si} = 7.4 \pm 0.4$ ns and $\tau_f = 37 \pm 1.1$ ns. This corresponds to an extra bandwidth added by the statistical interaction with the cesium atoms of $\Gamma_{meas} = 4.3 \pm 0.3$ MHz, in good agreement with the natural linewidth of $\Gamma_{lit} \approx 4.58$ MHz of the Cs D1 line. We measured a Klyshko efficiency of 8.4% for the idler photons and 0.067% for the re-emitted signal photons from fluorescence. Here, an improved collection efficiency of the photons [26] could enhance the Klyshko efficiency and lower the measurement time (see Fig. 5), both by orders of magnitude.

The maximum of the correlation function from heralded fluorescence is delayed with respect to the reference measurement presented in Fig. 5(a) by $\Delta\tau \approx 10$ ns, agreeing well with $\tau_{max}(\tau_{si}, \tau_f) = \frac{\tau_{si} \cdot \tau_f}{\tau_{si} - \tau_f} \cdot \ln(2\tau_{si}/(\tau_{si} + \tau_f))$ given by our model. The observed delay is typical for the response of a damped oscillator driven by a pulse. A similar response is observed in optical resonators [52].

5. CONCLUSION

We have demonstrated tunable and efficient interaction of two narrowband atomic resonances with photons created via SPDC in a WGMR. Our system offers both tunability and purity of the generated photons. The stringent phase-matching conditions of this triply resonant cavity allow single-mode operation without narrowband filtering. Going below the threshold of our optical parametric oscillations, we measured nearly complete absorption of the signal photons at the D1 lines of rubidium and cesium. The stability and brightness of our source greatly reduce the respective measurement times. This enables a direct probing of cesium D1 hyperfine levels with signal photons from fluorescence heralded by idler photons in a telecom band. To achieve this, we employed novel tuning mechanisms introduced with an evaluation of the mode spectrum and frequency shift based on a movable dielectric substrate. Future applications of this source involve the generation of photon pairs and squeezed light in combination with resonant systems such as quantum dots, single atoms, or optomechanical resonances. Multiphoton transitions are easily accessible via the resonator-enhanced SPDC process. Further studies may also include different materials for the WGMR beyond lithium niobate to cover transitions with shorter wavelengths and to study phase-matching configurations other than type I.

REFERENCES

1. H. J. Kimble, "The quantum internet," Nature **453**, 1023–1030 (2008).
2. E. Knill, R. Laflamme, and G. J. Milburn, "A scheme for efficient quantum computation with linear optics," Nature **409**, 46–52 (2001).
3. A. I. Lvovsky, B. C. Sanders, and W. Tittel, "Optical quantum memory," Nat. Photonics **3**, 706–714 (2009).
4. C. Simon, M. Afzelius, J. Appel, A. Boyer de la Giroday, S. J. Dewhurst, N. Gisin, C. Y. Hu, F. Jelezko, S. Kröll, J. H. Müller, J. Nunn, E. S. Polzik, J. G. Rarity, H. De Riedmatten, W. Rosenfeld, A. J. Shields, N. Sköld, R. M. Stevenson, R. Thew, I. A. Walmsley, M. C. Weber, H. Weinfurter, J. Wrachtrup, and R. J. Young, "Quantum memories," Eur. Phys. J. D **58**, 1–22 (2010).
5. M. Aspelmeyer, T. J. Kippenberg, and F. Marquardt, "Cavity optomechanics," Rev. Mod. Phys. **86**, 1391–1452 (2014).
6. H. P. Specht, C. Nölleke, A. Reiserer, M. Uphoff, E. Figueroa, S. Ritter, and G. Rempe, "A single-atom quantum memory," Nature **473**, 190–193 (2011).
7. J. Hald, J. L. Sørensen, C. Schori, and E. S. Polzik, "Spin squeezed atoms: a macroscopic entangled ensemble created by light," Phys. Rev. Lett. **83**, 1319–1322 (1999).
8. K. Hammerer, E. Polzik, and J. Cirac, "Teleportation and spin squeezing utilizing multimode entanglement of light with atoms," Phys. Rev. A **72**, 052313 (2005).

9. N. Sangouard, C. Simon, H. de Riedmatten, and N. Gisin, "Quantum repeaters based on atomic ensembles and linear optics," Rev. Mod. Phys. **83**, 33–80 (2011).

10. L. M. Duan, M. D. Lukin, J. I. Cirac, and P. Zoller, "Long-distance quantum communication with atomic ensembles and linear optics," Nature **414**, 413–418 (2001).

11. N. Gisin and R. Thew, "Quantum communication," Nat. Photonics **1**, 165–171 (2007).

12. M. D. Eisaman, J. Fan, A. Migdall, and S. V. Polyakov, "Review article: single-photon sources and detectors," Rev. Sci. Instrum. **82**, 071101 (2011).

13. M. Förtsch, G. Schunk, J. U. Fürst, D. Strekalov, T. Gerrits, M. J. Stevens, F. Sedlmeir, H. G. L. Schwefel, S. W. Nam, G. Leuchs, and C. Marquardt, "Highly efficient generation of single-mode photon pairs from a crystalline whispering-gallery-mode resonator source," Phys. Rev. A **91**, 023812 (2015).

14. M. Förtsch, J. U. Fürst, C. Wittmann, D. Strekalov, A. Aiello, M. V. Chekhova, C. Silberhorn, G. Leuchs, and C. Marquardt, "A versatile source of single photons for quantum information processing," Nat. Commun. **4**, 1818 (2013).

15. Z. Y. Ou and Y. J. Lu, "Cavity enhanced spontaneous parametric down-conversion for the prolongation of correlation time between conjugate photons," Phys. Rev. Lett. **83**, 2556–2559 (1999).

16. S. Fasel, O. Alibart, S. Tanzilli, P. Baldi, A. Beveratos, N. Gisin, and H. Zbinden, "High-quality asynchronous heralded single-photon source at telecom wavelength," New J. Phys. **6**, 163 (2004).

17. A. B. U'Ren, C. Silberhorn, K. Banaszek, and I. A. Walmsley, "Efficient conditional preparation of high-fidelity single photon states for fiber-optic quantum networks," Phys. Rev. Lett. **93**, 093601 (2004).

18. A. Fedrizzi, T. Herbst, A. Poppe, T. Jennewein, and A. Zeilinger, "A wavelength-tunable fiber-coupled source of narrowband entangled photons," Opt. Express **15**, 15377–15386 (2007).

19. M. Scholz, L. Koch, and O. Benson, "Statistics of narrow-band single photons for quantum memories generated by ultrabright cavity-enhanced parametric down-conversion," Phys. Rev. Lett. **102**, 063603 (2009).

20. F. Wolfgramm, Y. A. de Icaza Astiz, F. A. Beduini, A. Cerè, and M. W. Mitchell, "Atom-resonant heralded single photons by interaction-free measurement," Phys. Rev. Lett. **106**, 053602 (2011).

21. G. Harder, V. Ansari, B. Brecht, T. Dirmeier, C. Marquardt, and C. Silberhorn, "An optimized photon pair source for quantum circuits," Opt. Express **21**, 13975–13985 (2013).

22. J. Fekete, D. Rieländer, M. Cristiani, and H. de Riedmatten, "Ultranarrow-band photon-pair source compatible with solid state quantum memories and telecommunication networks," Phys. Rev. Lett. **110**, 220502 (2013).

23. C. Söller, B. Brecht, P. J. Mosley, L. Y. Zang, A. Podlipensky, N. Y. Joly, P. S. J. Russell, and C. Silberhorn, "Bridging visible and telecom wavelengths with a single-mode broadband photon pair source," Phys. Rev. A **81**, 031801 (2010).

24. W. Liang, A. A. Savchenkov, Z. Xie, J. F. McMillan, J. Burkhart, V. S. Ilchenko, C. W. Wong, A. B. Matsko, and L. Maleki, "Miniature multioctave light source based on a monolithic microcavity," Optica **2**, 40–47 (2015).

25. A. Kuhn, M. Hennrich, and G. Rempe, "Deterministic single-photon source for distributed quantum networking," Phys. Rev. Lett. **89**, 067901 (2002).

26. R. Maiwald, A. Golla, M. Fischer, M. Bader, S. Heugel, B. Chalopin, M. Sondermann, and G. Leuchs, "Collecting more than half the fluorescence photons from a single ion," Phys. Rev. A **86**, 043431 (2012).

27. T. Utikal, E. Eichhammer, L. Petersen, A. Renn, S. Götzinger, and V. Sandoghdar, "Spectroscopic detection and state preparation of a single praseodymium ion in a crystal," Nat. Commun. **5**, 3627 (2014).

28. B. Lounis and W. E. Moerner, "Single photons on demand from a single molecule at room temperature," Nature **407**, 491–493 (2000).

29. P. Siyushev, G. Stein, J. Wrachtrup, and I. Gerhardt, "Molecular photons interfaced with alkali atoms," Nature **509**, 66–70 (2014).

30. C. Kurtsiefer, S. Mayer, P. Zarda, and H. Weinfurter, "Stable solid-state source of single photons," Phys. Rev. Lett. **85**, 290–293 (2000).

31. P. Michler, A. Kiraz, C. Becher, W. V. Schoenfeld, P. M. Petroff, L. Zhang, E. Hu, and A. Imamoglu, "A quantum dot single-photon turnstile device," Science **290**, 2282–2285 (2000).

32. C. Santori, D. Fattal, J. Vučković, G. S. Solomon, and Y. Yamamoto, "Indistinguishable photons from a single-photon device," Nature **419**, 594–597 (2002).

33. A. Kuzmich, W. P. Bowen, A. D. Boozer, A. Boca, C. W. Chou, L.-M. Duan, and H. J. Kimble, "Generation of nonclassical photon pairs for scalable quantum communication with atomic ensembles," Nature **423**, 731–734 (2003).

34. B. Srivathsan, G. K. Gulati, B. Chng, G. Maslennikov, D. Matsukevich, and C. Kurtsiefer, "Narrow band source of transform-limited photon pairs via four-wave mixing in a cold atomic ensemble," Phys. Rev. Lett. **111**, 123602 (2013).

35. L. Zhao, X. Guo, C. Liu, Y. Sun, M. Loy, and S. Du, "Photon pairs with coherence time exceeding 1 μs," Optica **1**, 84–88 (2014).

36. G. Schunk, J. U. Fürst, M. Förtsch, D. V. Strekalov, U. Vogl, F. Sedlmeir, H. G. L. Schwefel, G. Leuchs, and C. Marquardt, "Identifying modes of large whispering-gallery mode resonators from the spectrum and emission pattern," Opt. Express **22**, 30795–30806 (2014).

37. J. Fürst, D. Strekalov, D. Elser, A. Aiello, U. Andersen, C. Marquardt, and G. Leuchs, "Quantum light from a whispering-gallery-mode disk resonator," Phys. Rev. Lett. **106**, 113901 (2011).

38. J. Fürst, D. V. Strekalov, D. Elser, M. Lassen, U. L. Andersen, C. Marquardt, and G. Leuchs, "Naturally phase-matched second-harmonic generation in a whispering-gallery-mode resonator," Phys. Rev. Lett. **104**, 153901 (2010).

39. I. Breunig, B. Sturman, F. Sedlmeir, H. G. L. Schwefel, and K. Buse, "Whispering gallery modes at the rim of an axisymmetric optical resonator: analytical versus numerical description and comparison with experiment," Opt. Express **21**, 30683–30692 (2013).

40. Y. Demchenko and M. Gorodetsky, "Analytical estimates of eigenfrequencies, dispersion, and field distribution in whispering gallery resonators," J. Opt. Soc. Am. B **30**, 3056–3063 (2013).

41. J. U. Fürst, D. V. Strekalov, D. Elser, A. Aiello, U. L. Andersen, C. Marquardt, and G. Leuchs, "Low-threshold optical parametric oscillations in a whispering gallery mode resonator," Phys. Rev. Lett. **105**, 263904 (2010).

42. C. S. Werner, T. Beckmann, K. Buse, and I. Breunig, "Blue-pumped whispering gallery optical parametric oscillator," Opt. Lett. **37**, 4224–4226 (2012).

43. G. Kozyreff, J. L. Dominguez Juarez, and J. Martorell, "Whispering-gallery-mode phase matching for surface second-order nonlinear optical processes in spherical microresonators," Phys. Rev. A **77**, 043817 (2008).

44. T. Debuisschert, A. Sizmann, E. Giacobino, and C. Fabre, "Type-II continuous-wave optical parametric oscillators oscillation and frequency-tuning characteristics," J. Opt. Soc. Am. B **10**, 1668–1680 (1993).

45. D. A. Steck, "Rubidium 85 D line data, rubidium 87 D line data, cesium D line data," Technical Report (Los Alamos National Laboratory, 2008), available at http://steck.us/alkalidata.

46. W. L. Bond, "Measurement of the refractive indices of several crystals," J. Appl. Phys. **36**, 1674–1677 (1965).

47. S. M. George, "Atomic layer deposition: an overview," Chem. Rev. **110**, 111–131 (2010).

48. I. Teraoka and S. Arnold, "Theory of resonance shifts in TE and TM whispering gallery modes by nonradial perturbations for sensing applications," J. Opt. Soc. Am. B **23**, 1381–1389 (2006).

49. V. S. Ilchenko, A. B. Matsko, A. A. Savchenkov, and L. Maleki, "Low-threshold parametric nonlinear optics with quasi-phase-matched whispering-gallery modes," J. Opt. Soc. Am. B **20**, 1304–1308 (2003).

50. T. Beckmann, K. Buse, and I. Breunig, "Optimizing pump threshold and conversion efficiency of whispering gallery optical parametric oscillators by controlled coupling," Opt. Lett. **37**, 5250–5252 (2012).

51. D. N. Klyshko, "Use of two-photon light for absolute calibration of photoelectric detectors," Sov. J. Quantum Electron. **10**, 1112–1117 (1980).

52. M. Bader, S. Heugel, A. L. Chekhov, M. Sondermann, and G. Leuchs, "Efficient coupling to an optical resonator by exploiting time-reversal symmetry," New J. Phys. **15**, 123008 (2013).